Spatiotemporal Control of Light Transmission through a Multimode Fiber with Strong Mode Coupling

Wen Xiong, Philipp Ambichl, Yaron Bromberg, Brandon Redding, Stefan Rotter, and Hui Cao

Phys. Rev. Lett. **117**, 053901 — Published 25 July 2016

DOI: 10.1103/PhysRevLett.117.053901

Spatiotemporal Control of Light Transmission through a Multimode Fiber with Strong Mode Coupling

Wen Xiong[1], Philipp Ambichl[2], Yaron Bromberg[1], Brandon Redding[1], Stefan Rotter[2], Hui Cao[1*]
[1]*Applied Physics Department, Yale University, New Haven CT 06520, USA*
[2]*Institute for Theoretical Physics, Vienna University of Technology, A-1040 Vienna, Austria*

We experimentally generate and characterize eigenstates of the Wigner-Smith time-delay matrix, called principal modes, in a multimode fiber with strong mode coupling. The unique spectral and temporal properties of principal modes enable global control of temporal dynamics of optical pulses transmitted through the fiber, despite random mode mixing. Our analysis reveals that well-defined delay times of the eigenstates are formed by multi-path interference, which can be effectively manipulated by spatial degrees of freedom of input wavefronts. This study is essential to controlling dynamics of wave scattering, paving the way for coherent control of pulse propagation through complex media.

PACS numbers: 42.65.Sf, 42.25.-p, 42.81.Cn

Temporal dynamics of wave scattering in complex systems has been widely studied in quantum mechanics, nuclear physics, acoustics and optics. Most of these studies, e.g., electromagnetic or ultrasonic wave propagation in billiards [1–4], electron transport through quantum dots [5, 6], and light scattering in random media [7–12] focused on statistics of delay times, i.e., eigenvalues of the Wigner-Smith time-delay matrix [13–15]. Despite innumerable trajectories waves could take through an open complex system, an eigenstate of the Wigner-Smith matrix remarkably has a well-defined delay time. Some of the eigenstates are particlelike with their wavefunctions concentrating on a single trajectory [4], and hence a definite transit time is expected. Most of the states, however, consist of enormous trajectories with various lengths such that it is concealed how well-defined delay times can be attributed to these states.

Largely in parallel, the Wigner-Smith eigenstates were introduced for multimode optical fibers (MMFs), which recently attracted much attention due to the rapid development of space-division multiplexing for telecommunications [16]. Inherent imperfections and external perturbations introduce random mode coupling and cause pulse broadening and distortion in a MMF. As a generalization of principal states of polarization in single-mode fibers [17], the Wigner-Smith eigenstates, also called principal modes (PMs) in MMFs, were proposed to suppress modal dispersion [18].

Advances in wavefront shaping techniques now make it possible to probe a single Wigner-Smith eigenstate in optics. Recently PMs were observed in a MMF with weak mode coupling [19]. In this regime, mode coupling in the fiber is only perturbative and PMs are similar to eigenmodes of a perfect fiber [23]. In the strong mode coupling regime, however, all modes are strongly mixed. Multiple scattering of light between different modes generates numerous paths for light to propagate through the fiber. It thus remains obscure how PMs are formed with well-defined delay times and what properties they possess in the presence of non-perturbative mode mixing.

In this letter, we report on a demonstration of PMs in a MMF with strong mode coupling. Our analysis uncovers that well-defined delay times of PMs can be explained by multi-path interference that is tailored by spatial degrees of freedom of the input wavefront. This multi-path interference also determines spectral bandwidths of PMs, which limits the temporal width of pulses that can be transmitted through the fiber without distortion.

The Wigner-Smith time-delay matrix is defined as $Q \equiv -iS^{-1}dS/d\omega$, where S is the scattering matrix [14, 15]. In the absence of backscattering in the fiber, it can be expressed as $Q \equiv -iT^{-1}dT/d\omega$ [18, 20], in which S is replaced by the transmission matrix T. We experimentally measure the spectrally-resolved field transmission matrix of a step-index MMF in an off-axis holographic setup shown schematically in Fig. 1(a). To introduce strong mode coupling in this one-meter-long fiber, we apply stress to it with clamps. Field transmission matrices are measured in momentum space and converted to mode space. Figure 1(b) shows the amplitude of a measured transmission matrix. Regardless of the mode light is launched into, the output field spreads over all modes, although higher order modes have lower amplitudes due to stronger loss. The transmission matrix is different from that in the weak coupling regime, which has larger elements closer to the matrix diagonal, confirming the strong mode coupling in the current fiber.

The time-delay matrix Q is constructed from the spectrally-resolved transmission matrix. Eigenvectors of Q give input fields for PMs. They are unique input states with first-order frequency derivatives of their output fields vanishing at a certain frequency [18]. In an ideal MMF, PMs are simply linearly polarized modes, which are eigenmodes of MMFs in the weak guiding approximation. In the weak mode coupling regime, the fiber is shorter than the correlation length (the distance beyond which the spatial profile becomes uncorrelated

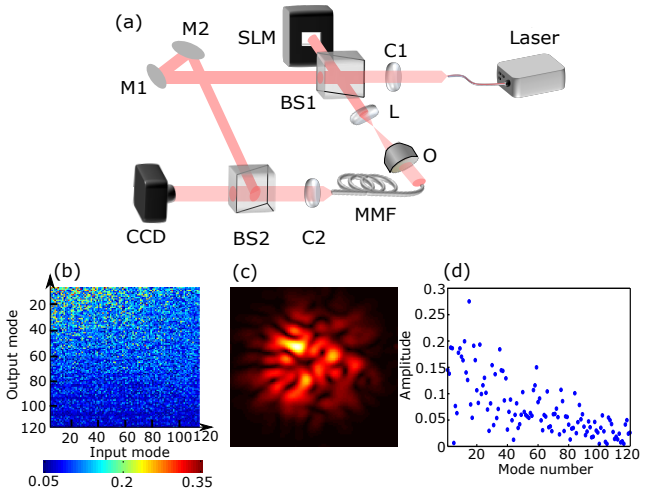

Figure 1. (color online) (a) Schematic of the experimental setup. The continuous-wave output of a tunable laser is collimated at C1, and split into two arms by a beam splitter (BS1). Light in one arm is modulated by the SLM and imaged to the fiber facet by a lens (L1) and an objective (O). The output field from the fiber is collected by a lens (C2) that one focal length away from the fiber facet and combined with light in the other arm at a second beam-splitter (BS2). By offsetting BS2 to introduce a phase tilt between the two wavefronts, interference fringes are formed. From the interferogram recorded by the camera (CCD) at the back focal plane of C2, the output field is extracted in momentum space. The mirrors (M1, M2) are used to match the path-length of the two arms. The MMF has 50 μm core diameter and 0.22 numerical aperture. (b) Amplitude of the measured transmission matrix at $\lambda = 1550$ nm (ω=1219 THz). (c) Amplitude profile of a PM at the output. (d) Decomposition of the PM in (c) by linearly polarized modes.

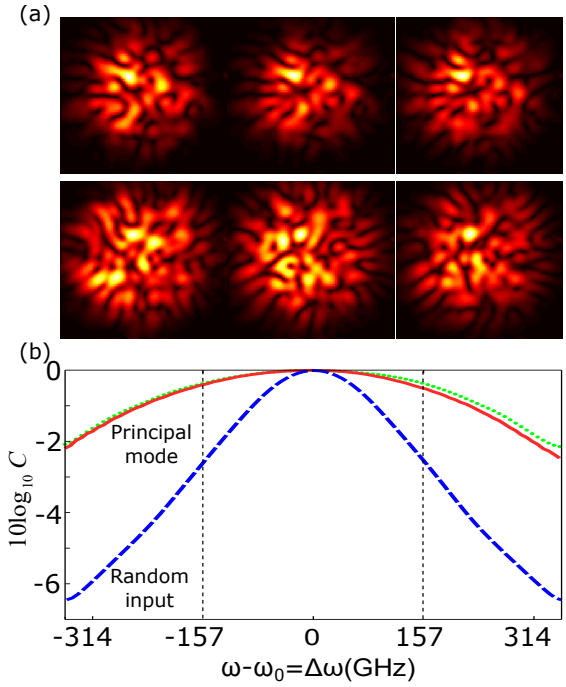

Figure 2. (color online) (a) Output field amplitude for a PM input with short delay time at $\omega_0 = 1219$ THz (top row), or a random superposition of linearly polarized modes (bottom row). The input frequency is $\omega - \omega_0 = -157$ GHz (left), 0 (middle), and 157 GHz (right). The output fields for the PM input are similar while those for random input are totally different. (b) Spectral correlation function $C(\Delta\omega)$ of the output field, experimentally measured for a PM (red solid), and calculated from the transmission matrix and input wavefront of the same PM (green dotted). For comparison, $C(\Delta\omega)$ for a random input is also shown (blue dashed). $C(\Delta\omega)$ is normalized to one at $\Delta\omega = 0$. Its value decreases to 0.9 at $\Delta\omega = 338$ GHz for the PM and 173 GHz for the random input. The agreement between the red and green curves illustrates the accuracy of the measurement.

[21]), and each PM consists of a few modes with similar propagation constants [23]. However, if the fiber length well exceeds the correlation length, all modes are thoroughly mixed and PMs are expected to be distinct from those in the weak coupling regime.

We use a spatial light modulator (SLM) to generate input wavefronts of individual PMs in this MMF with strong mode coupling. To modulate amplitude and phase of the input field with the phase-only SLM, a computer-generated phase hologram is employed [22]. Figure 1(c) shows the output pattern of a PM, which is speckled and does not resemble any linearly polarized mode. Modal decomposition of the output field reveals that the PM is a mixture of many modes [Fig. 1(d)], in contrast to PMs in the weak mode coupling regime [23].

To investigate the spectral property of PMs, we scan the frequency ω while keeping the input field to that of a PM at ω_0. Figure 2(a) shows the nearly identical far-field patterns of the PM at three different frequencies (top row). For comparison, a random superposition of modes at the input results in different output profiles at these frequencies [bottom row of Fig. 2(a)]. This striking difference illustrates the slower spectral decorrelation of a PM.

To be quantitative, we calculate the spectral correlation function $C(\Delta\omega \equiv \omega - \omega_0) \equiv |\mathbf{\Psi}(\omega_0)^* \cdot \mathbf{\Psi}(\omega)|$, where $\mathbf{\Psi}(\omega)$ is a vector representing the output fields in all spatial channels with its magnitude normalized to unity. As shown in Fig. 2(b), $C(\Delta\omega)$ for the PM is significantly larger than that for the random input. It displays a broad plateau at $\Delta\omega = 0$. To understand the shape of the correlation curve, we denote $C(\Delta\omega) = \cos[\theta(\Delta\omega)]$ [23], where θ is the angle between the two output field vectors at ω and ω_0. Since $\theta(0) = 0$, the first-order derivative of C with respect to $\Delta\omega$ vanishes at $\Delta\omega = 0$ for any input wavefront. The second-order derivative at $\Delta\omega = 0$ is proportional to $[\theta'(0)]^2$, where $\theta' \equiv d\theta/d\Delta\omega$. For PMs, $\theta'(0) = 0$, because the output field remains unchanged to the first order of frequency variation. Thus the second-order derivative vanishes for PMs, leading to a plateau,

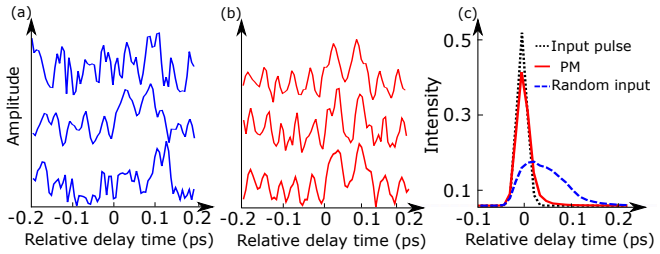

Figure 3. (color online) (a,b) Temporal variation of the output field amplitude in three spatial channels (three speckles grains) when an optical pulse is spatially launched into a random superposition of modes (a) or a PM at $\omega_0 = 194$ THz (b). The output field is recorded in a frequency range of 400 GHz with a step size of 2.5 GHz. The Fourier transform is performed to obtain the temporal evolution of the field. The horizontal axis is the relative delay time, obtained by subtracting the average delay time for random inputs. The temporal traces of individual spatial channels are totally different for the random input, but nearly identical for the PM input. (c) Spatially integrated intensity of the input (black dotted) and the output pulses when a Gaussian pulse is injected to the MMF with random spatial profile (blue dashed) or with the profile of a PM (red solid).

which is absent for random inputs, at the center of the correlation curve.

Next, we probe temporal dynamics of a single PM. The transmission of a pulse through a MMF with strong mode coupling involves spatial and temporal distortions. Strong mode mixing results in the hop of light among modes with different propagation constants. Thus light can take many paths of varying lengths through the fiber. The output field in each spatial channel (e.g. speckle grain) is a sum of waves with different paths, each associated with a respective time delay, leading to temporal broadening and distortion of the input pulse. Typically, temporal traces vary from one channel to another, since combinations of paths differ. This is confirmed by simulating the propagation of a pulse, $\phi(t) = \int \phi(\omega)\, e^{-i\omega t} d\omega$, with a spectrum $\phi(\omega)$. Light is spatially launched into a random superposition of modes at the input, and the output fields are experimentally recorded at multiple frequencies. We perform the Fourier transform to obtain the temporal evolution of the output field in each spatial channel. Figure 3(a) shows temporal traces of the field amplitude in three spatial channels. They differ from each other, due to strong mode scrambling in the fiber.

However, when input light is spatially coupled to a PM, the output fields in all spatial channels are synchronized, as shown in Fig. 3(b). This is a direct consequence of the invariance of the output field with frequency. Specifically, the output field vector at frequency ω can be written as $\mathbf{\Psi}(\omega) = \phi(\omega)T(\omega)\mathbf{\Phi}$, where $\mathbf{\Phi}$ corresponds to a PM input at ω_0. If the input pulse bandwidth is less than the spectral correlation width of the PM, $T(\omega)\mathbf{\Phi} \approx \alpha(\omega)\hat{\mathbf{\Psi}}_0$, where $\hat{\mathbf{\Psi}}_0$ is a unit vector representing the normalized output field for the PM at ω_0, and $\alpha(\omega)$ is a complex number that may vary with frequency. The Fourier transform of $\mathbf{\Psi}(\omega)$ can be written as $\mathbf{\Psi}(t) = \tilde{\phi}(t)\hat{\mathbf{\Psi}}_0$, where $\tilde{\phi}(t) = \int \phi(\omega)\alpha(\omega)e^{-i\omega t}dt$ represents the temporal shape of the output pulse. Hence, spatial and temporal variations of the output field become decoupled for PMs. The temporal traces in all output channels are identical up to a constant factor given by the elements of $\hat{\mathbf{\Psi}}_0$. The spatial profile of the output field remains constant in time, allowing the spatial and temporal distortions to be corrected separately. For example, the output pulse shape can be tailored by modulating the spectral phase of the input spectrum $\phi(\omega)$. Since the output fields are spatially coherent, a spatial mask can convert the output to any desired pattern or focus to a diffraction-limited spot.

Let us consider a simple case, $\alpha(\omega) \simeq \alpha_0 e^{i\eta(\omega)}$, where α_0 is a constant amplitude and the phase $\eta(\omega) \simeq \eta(\omega_0) + \eta_0' (\omega - \omega_0)$, where η_0' is the value of $d\eta/d\omega$ at ω_0. The output pulse, $\tilde{\phi}(t) \propto \phi(t - \eta_0')$, has the same temporal shape as the input one. This is confirmed by synthesizing a pulse with Gaussian spectrum and flat phase at the input. The output intensity, summed over all spatial channels, is plotted in Fig. 3(c) together with the input pulse. The output pulse has negligible broadening and shape distortion, despite strong mode coupling in the fiber. In contrast, the same pulse, but with a random input pattern, suffers from severe broadening as seen in Fig. 3(c). PMs thus compensate for temporal distortions induced by modal dispersion in a MMF.

The unique spectral and temporal properties of PMs hold only within a finite frequency range. It is hence important to determine bandwidths of PMs. Since the spectral decorrelation of the output pattern for any input wavefront depends on fiber properties, such as fiber length and numerical aperture, we consider below the ratio of PM bandwidths to the average bandwidth of random inputs. Figure 4(a) plots the experimentally measured bandwidths of all PMs versus their delay times. The shorter the delay time, the larger the bandwidth.

To obtain a physical understanding of PMs and their spectral correlation widths, we resort to an intuitive picture of optical paths in the fiber. The output field is a result of interference of waves following innumerable possible trajectories in the MMF created by strong mode coupling. As the input frequency changes, relative phases accumulated along trajectories of different lengths vary, modifying the output field. Specifically, the output field in the m^{th} spatial channel can be written as $\Psi_m = \int u_m(l)dl$, where $u_m(l)$ is a sum of fields taking all possible paths with the same length l. With a small frequency detuning $\Delta\omega$, the output field becomes $\Psi_m(\Delta\omega) = \int u_m(l)e^{i\Delta\omega\, l/c}dl$, in the weak guiding approximation. Thus $u_m(l)$ can be obtained experimentally from the Fourier transform of $\Psi_m(\Delta\omega)$. Accounting for all spatial channels, $U(l) = \sum_m |u_m(l)|^2$ gives an intensity

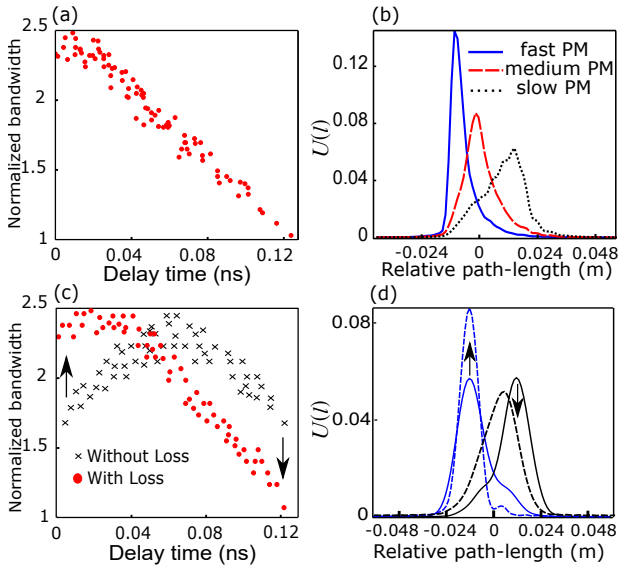

Figure 4. (color online) (a) Measured spectral correlation width $\Delta\omega_c$ of PMs with different delay times. $\Delta\omega_c$, given by $|C(\Delta\omega_c)| = 0.9|C(0)|$, is normalized by the average bandwidth of random inputs. The shortest delay time is set to 0. (b) Intensity distribution over the path-length $U(l)$ for three measured PMs with the delay time = 0, 0.06, 0.12 ns. The relative path-length l is obtained by subtracting the average path-length of random inputs. $U(l)$ is normalized: $\int U(l)\,dl = 1$. (c) Calculated spectral correlation width of the PMs with (red circles) and without (black crosses) mode-dependent loss. (d) Intensity distribution over the path-length for two PMs with the delay time = 0 ns (blue), 0.12 ns (black), in the presence (dashed) or absence (solid) of mode-dependent loss. The mode-dependent loss narrows (broadens) the path-length distribution for the fast (slow) principle mode, thereby increasing (reducing) the spectral correlation width.

distribution over path-lengths, which is determined by the input wavefront.

Figure 4(b) compares $U(l)$ for three PMs with different delay times. The fast PM concentrated the intensity on shorter paths. Although the waves can take many longer paths, destructive interference of longer paths makes $U(l)$ vanish. The opposite happens to the slow PM. The redistribution of intensity among different path-lengths is determined by the input wavefront. Therefore, delay times in a MMF with strong mode coupling is determined by multi-path interference, which can be effectively controlled by spatial degrees of freedom of the input wavefront. We emphasize that the well-defined delay times for PMs are only guaranteed at the output end of the fiber, such that PM-based pulses spread in the middle of the fiber before recompressing again at the output. This behavior is in sharp contrast to that of particle-like states [23, 24].

The intensity distribution over path-lengths also determines the spectral correlation widths of PMs. The narrower the distribution, the weaker the dephasing between different path-lengths by frequency detuning, and the smaller the change in the interference pattern at the output. Hence, PMs with shorter delay times have larger spectral correlation widths due to the narrower path-length distribution.

The final question we address here is why fast PMs have narrower path-length distributions. To answer this question, we perform numerical simulations using the concatenated waveguide model [25]. For simplicity, we consider a planar waveguide with a 300μm core and a 0.22 numerical aperture, supporting 86 modes. The waveguide is one meter and composed of 20 segments. Light propagates without mode coupling in each segment. Between adjacent segments, all modes are randomly coupled, as simulated by a unitary random matrix. To include mode-dependent loss, we introduce a uniform absorption coefficient to each segment. Higher-order modes with smaller propagation constants, have longer transit time, thus experiencing more attenuation. In terms of optical path, longer paths have more loss than shorter ones.

Figure 4(c) plots spectral correlation widths of PMs in the absence of mode-dependent loss (black crosses). The fast and slow PMs have almost identical bandwidth, as the corresponding intensity distribution among the path-length exhibits similar spread at different mean values [Fig. 4(d), solid curves]. With the introduction of mode-dependent loss, the bandwidth of fast PMs increases, while the bandwidth of slow ones decreases, leading to agreement with the experimental data [compare red dots in Fig. 4(a) with those in Fig. 4(c)]. This rearrangement can be explained by the change in $U(l)$ that is plotted in Fig. 4(d). The distribution for a fast PM, which concentrates on short paths, becomes narrower, because longer paths are further suppressed by loss. For a slow PM, the stronger attenuation of longer paths not only shifts the peak of $U(l)$ to smaller l, but also broadens the distribution. Qualitatively, the change of PM bandwidth induced by the mode-dependent loss is not sensitive to the kind of loss the fiber experiences, as long as higher-order modes have more loss, as expected for MMFs.

In summary, we experimentally probe individual eigenstates of the Wigner-Smith time-delay matrix of a MMF with strong mode coupling. We find that the well-defined delay times of the eigenstates are formed by multi-path interference, which can be manipulated by spatial degrees of freedom of the input wavefront. The multi-path interference also determines the frequency range over which the unique spectral and temporal properties of the Wigner-Smith eigenstates preserve. Within the bandwidth, spatial and temporal variations of the transmitted field are decoupled for the eigenstates, enabling a global spatiotemporal control of pulse transmission through complex media. Such global control, which is more challenging than control over a single spatial channel such as spatiotemporal focusing [26–31], has

potential applications in optical communication, imaging and sensing.

We acknowledge Chia Wei Hsu, Joel Carpenter and Nicolas Fontaine for interesting discussions. This work is supported partly by the US National Science Foundation under the Grant Nos. ECCS-1509361 and DMR-1205307. P.A. and S.R. acknowledge support by the Austrian Science Fund (FWF) through projects SFB NextLite (F49-P10) and project GePartWave(I1142).

* hui.cao@yale.edu

[1] E. Doron, U. Smilansky and A. Frenkel, Experimental demonstration of chaotic scattering of microwaves, Phys. Rev. Lett. **65**, 3072 (1990).

[2] D. V. Savin and H. J. Sommers, Delay times and reflection in chaotic cavities with absorption, Phys. Rev. E **68**, 036211 (2003).

[3] Y. V. Fyodorov, D. V. Savin and H. J. Sommers, Scattering, reflection and impedance of waves in chaotic and disordered systems with absorption, J. Phys. A **38**, 10731 (2005).

[4] S. Rotter, P. Ambichl and F. Libisch, Generating particlelike scattering states in wave transport, Phys. Rev. Lett. **106**, 120602 (2011).

[5] P. W. Brouwer, K. M. Frahm and C. W. J. Beenakker, Quantum mechanical time-delay matrix in chaotic scattering, Phys. Rev. Lett. **78**, 4737 (1997).

[6] P. W. Brouwer, K. M. Frahm and C. W. J. Beenakker, Distribution of the quantum mechanical time-delay matrix for a chaotic cavity, Waves Random Media **9**, 91 (1999).

[7] A. Lagendijk, and B. A. Van Tiggelen, Resonant multiple scattering of light, Phys. Rep. **270**, 143 (1996).

[8] A. Z. Genack, P. Sebbah, M. Stoytchev, and B. A. Van Tiggelen, Statistics of wave dynamics in random media, Phys. Rev. Lett. **82**, 715 (1999).

[9] B. A. Van Tiggelen, P. Sebbah, M. Stoytchev, and A. Z. Genack, Delay-time statistics for diffuse waves, Phys. Rev. E **59**, 7166 (1999).

[10] M. Davy, Z. Shi, J. Wang, X. Cheng, A. Z. Genack, Transmission eigenchannels and the densities of states of random media, Phys. Rev. Lett. **114**, 033901 (2015).

[11] Z. Shi and A. Z. Genack, Dynamic spectral properties of transmission eigenchannels in random media, Phys. Rev. B **92**, 184202 (2015).

[12] M. Mounaix, D. Andreoli, H. Defienne, G. Volpe, O. Katz, S. Grésillon and S. Gigan, Spatiotemporal coherent control of light through a multiply scattering medium with the multi-spectral transmission matrix, arXiv:1512.07753

[13] L. Eisenbud, Ph.D. thesis, Princeton, 1948.

[14] E. P. Wigner, Lower limit for the energy derivative of the scattering phase shift, Phys. Rev. **98**, 145 (1955).

[15] F. T. Smith, Lifetime matrix in collision theory, Phys. Rev. **118**, 349 (1960).

[16] D. J. Richardson, J. M. Fini and L. E. Nelson, Space-division multiplexing in optical fibres, Nature Photon. 7, 354 (2013)

[17] C. D. Poole and R. E. Wagner, Phenomenological approach to polarisation dispersion in long single-mode fibres, Electron. Lett. **22**, 1029 (1986).

[18] S. Fan and J. M. Kahn, Principal modes in multimode waveguides, Opt. Lett. **30**, 135 (2005).

[19] J. Carpenter, B. J. Eggleton and J. Schröder, Observation of Eisenbud-Wigner-Smith states as principal modes in multimode fibre, Nature Photon. **9**, 751 (2015)

[20] A. A. Juarez, C. A. Bunge, S. Warm and K. Petermann, Perspectives of principal mode transmission in mode-division-multiplex operation, Opt. Express **20**, 13810 (2012).

[21] K. P. Ho and J. M. Kahn, Linear propagation effects in mode-division multiplexing systems, J. Lightwave Technol. **32**, 614 (2014)

[22] V. Arrizón, U. Ruiz, R. Carrada and L. A. González, Pixelated phase computer holograms for the accurate encoding of scalar complex fields, J. Opt. Soc. Am. A **24**, 3500 (2007).

[23] See Supplemental Material for the comparison of principal modes in weak and strong mode coupling regimes, the detailed discussion of the spectral correlation function, the numerical simulation of the effect of polarizations and the comparison of principal modes and particle-like states.

[24] B. Gérardin, J. Laurent, P. Ambichl, C. Prada, S. Rotter, A. Aubry, Particle-like wave packets in complex scattering systems, arXiv:1602.05812.

[25] K. P. Ho and J. M. Kahn, Statistics of group delays in multimode fiber with strong mode coupling, J. Lightwave Technol. **29**, 3119 (2011).

[26] O. Katz, E. Small, Y. Bromberg and Y. Silberberg, Focusing and compression of ultrashort pulses through scattering media, Nature Photon. **5**, 372 (2011).

[27] D. J. McCabe, A. Tajalli, D. R. Austin, P. Bondareff, I. A. Walmsley, S. Gigan and B. Chatel, Spatio-temporal focusing of an ultrafast pulse through a multiply scattering medium. Nat. Commun.**2**, 447 (2011).

[28] J. Aulbach, B. Gjonaj, P. M. Johnson, A. P. Mosk and A. Lagendijk, Control of light transmission through opaque scattering media in space and time, Phys. Rev. Lett. **106**, 103901 (2011).

[29] J. Aulbach, B. Gjonaj, P. M. Johnson and A. Lagendijk, Spatiotemporal focusing in opaque scattering media by wave front shaping with nonlinear feedback. Opt. Express **20**, 29237 (2012).

[30] Z. Shi, M. Davy, J. Wang and A. Z. Genack, Focusing through random media in space and time: a transmission matrix approach, Opt. Lett. **38**, 2714 (2013).

[31] E. E. Morales-Delgado, S. Farahi, I. N. Papadopoulos, D. Psaltis and C. Moser, Delivery of focused short pulses through a multimode fiber, Opt. Express **23**, 9109 (2015).